SEISMIC NOISE-BASED METHODS FOR SOFT-ROCK LANDSLIDE CHARACTERIZATION

Ombeline Méric[1, 2], Stéphane Garambois[1], Jean-Philippe Malet[3], Héloise Cadet[4, 5], Philippe Guéguen[4] and Denis Jongmans[1]

[1] LIRIGM-LGIT, Maison des Géosciences, Université Joseph Fourier,
BP 53, F-38041 Grenoble Cedex 9, France.
Tel: +33 (0)476 828 046
e-mail: ombeline.meric@ujf-grenoble.fr

[2] SAGE, ZI de Mayencin, BP 17 – F-38610 Gières, France, Tel: +33 (0)476 447 572

[3] Faculty of Geosciences, UCEL, Utrecht University, Heidelberglaan 2, Po.Box 80.115, NL-3508 TC Utrecht, The Netherlands

[4] LGIT, Maison des Géosciences, Université Joseph Fourier,
BP 53, 38041 Grenoble Cedex 9, France.

[5] CETE Méditerranée, Laboratoire Régional de Nice
56, Boulevard Stalingrad, F-06359 Nice Cedex 4, France

Keywords: seismic noise, soft rock landslide, *in-situ* characterization, 3D geometry

ABSTRACT

In order to better understand the mechanics and dynamic of landslides, it is of primary interest to image correctly their internal structure. Several active geophysical methods are able to provide the geometry of a given landslide, but were rarely applied in 3 dimensions in the past. The main disadvantages of methods like seismic reflection or electrical tomographies are that there are heavy to set up, require for some heavy processing tools to implement, and consequently are expensive and time consuming. Moreover, in the particular case of soft-rock landslides, their respective sensitivity and resolution are not always adequate to locate the potential slip surfaces. The passive methods, which require lighter instrumentation and easier processing tools, can represent an interesting alternative, particularly for difficult accessible landslides. Among them, the seismic noise based methods have shown increasing applications and developments, in particular for seismic hazard mapping in urban environment. In this paper, we present seismic noise investigations carried out on two different sites, a mudslide and a translational clayey landslide where independent measurements (geotechnical and geophysical tests) were performed earlier. Our investigations were composed of H/V measurements, which are fast and easy to perform in the field, in order to image shear wave contrasts (slip surfaces), and seismic noise array method, which is heavier to apply and interpret, but provides S-waves velocity profile versus depth. The comparisons between geophysical investigations and geotechnical information proved the applicability of such passive methods in 3D complexes, but also some limitations. Indeed interpretation of these measurements can be tricky in rough and non-homogeneous terrains.

CARACTERISATION DE GLISSEMENTS ARGILEUX PAR DES METHODES DE BRUIT DE FOND SISMIQUE

Mots clés : bruit de fond sismique, glissement argileux, caractérisation in-situ, géométrie 3D

RESUME

Afin d'identifier les mécanismes de contrôle et de caractériser la dynamique de glissements de terrain, il est impératif d'imager correctement leur structure interne. Plusieurs méthodes géophysiques actives sont utilisables pour identifier la géométrie d'un glissement de terrain, mais leurs potentialités ont été rarement testées dans des environnements fortement 3D. Les principaux inconvénients de méthodes géophysiques telles que la sismique réflexion ou la tomographie électrique sont la difficulté de mise en œuvre et la complexité des traitements de données, ce qui les rend chères et consommatrices en temps. De plus, pour le cas particulier de glissements argileux, leur sensibilité et résolution ne sont pas toujours adaptées à la détection des surfaces de glissement. Les méthodes géophysiques passives, qui offrent l'avantage d'une instrumentation légère et d'un traitement des données plus simple, représentent ainsi une alternative intéressante, particulièrement pour des sites difficiles d'accès. Parmi celles-ci, les méthodes de bruit sismique ambiant connaissent depuis quelques années des développements et applications intéressants, notamment pour le zonage de l'aléa sismique en milieu urbain. Nous présentons dans ce papier des investigations par bruit de fond sismique effectuées sur deux sites instables, un glissement-coulée et un glissement translationnel, où des investigations géotechniques et géophysiques indépendantes ont été réalisées. Nos investigations se composent (1) de mesures H/V, simples, légères et rapides à

1 installer sur site, afin de cartographier des contrastes de vitesse d'onde S (surface de
2 glissement) et de (2) de mesures de bruit de fond réseau, plus délicate et complexe à déployer
3 sur site et à interpréter, mais qui permet d'accéder à des profils de vitesses d'ondes S en
4 fonction de la profondeur. Les comparaisons entre nos investigations géophysiques et les
5 sondages géotechniques prouvent l'applicabilité des méthodes géophysiques passives dans
6 des environnements 3D, mais indiquent également certaines limites. En effet, l'interprétation
7 des données peut s'avérer difficile dans des terrains hétérogènes et à forte rugosité.
8

INTRODUCTION

The authorities with the responsibility of protecting livelihood and infrastructure from the threat of landslide hazard must be particularly concerned with three critical aspects: (1) the spatial distribution of the processes, (2) the understanding of their mechanisms, (3) their magnitude and temporal frequency. These purposes imply to accurately assess the characteristics of the landslides and to evaluate their controlling factors (climate, seismology) in a dynamic dimension. For these reasons, 2D and 3D mathematical models have been developed during the last decade in order to simulate the complexity of landslide mechanisms [Commend et al., 2004; Malet et al., 2005; Tacher et al., 2005]. At this time, one of their main weaknesses lies in the large uncertainty of parameters describing the unstable area. For example, critical information, such as the 3D geometry of a landslide and of its surrounding geology, its geomechanical and hydrological properties, or its internal discontinuities, as well as the uncertainties associated to these parameters are rarely available.

Landslides are generally studied using geotechnical investigations (boreholes, penetrometric tests, etc), local instrumentation placed in boreholes (piezometers, inclinometers), as well as detailed geomorphological observations [Giraud et al., 1991; Flageollet et al., 2004]. Even if these studies are essential because they provide direct information of the landslide material, their cost and limited spatial representativeness hinder their use for 3D studies. In particular, except by multiplying the number of tests, these methods are not able to image the lateral variability of landslide characteristics. To address this problem, a large choice of geophysical methods is available on a broad spatial scale. An increasing trend to apply geophysical studies for landslides characterization has been recently observed, mainly thanks to the improvement of data acquisition systems and of data inversion

softwares. A critical review of these methods is discussed by Jongmans and Garambois [2006, this issue], who point out the need of combining geophysical methods [see also Israil and Pachani, 2003] and of validating geophysical data by geotechnical information [Maquaire et al., 2001; Flageollet et al., 2004]. In practise, the high cost, time consuming efforts and difficulties in implementing 3D geophysical investigations can only be considered for active landslides presenting a high level of risk or for research purposes. Consequently, fast methods, easy to deploy and presenting lower costs have to be developed in the future, at least to locate the slip surfaces and characterize bedrock geometries in 3D. Methods based on seismic noise measurements, which were extensively applied for seismic hazard mapping in the recent years, fill close criteria [Asten, 2004].

In this paper, we present two examples of seismic noise investigations performed on two soft-rock landslides of the South French Alps (fig. 1), *ie.* the Super-Sauze mudslide in the black marls of the Ubaye valley and the Saint-Guillaume translational landslide in the varved clays of the Trièves region. At both sites, the slip surfaces are located within a homogeneous clay formation. The purposes of our studies are to evaluate the potential of seismological data, first to detect the slip surfaces using the H/V spectral ratio and second, to derive S-wave velocity profiles using seismic noise networks. To our knowledge, only a few seismic noise investigations were performed in the past on landslides. Galippolli et al. [2000] briefly mentioned the use of H/V methods on the large Giarossa landslide (southern Italy) which helped to interpret electrical tomography images. Recently, Méric et al [2005] failed to identify the slip surface of the large rocky landslide of Séchilienne using H/V measurements. They however noted a clear correlation between amplitude of the seismic noise and the landslide displacement rate explained by fracture density.

As both Super-Sauze and Saint-Guillaume landslides were characterized and monitored using geotechnical and geophysical measurements, a critical discussion of results provided by seismic noise methods is thus possible.

SEISMIC NOISE THEORY

The H/V method consists in computing the spectral ratio between horizontal and vertical components of the seismic noise recorded simultaneously at a given location with a 3D seismometer placed at the ground surface. Nogoshi & Igarashi [1972] first proposed the use of the H/V method as a tool for the estimate of the seismic response of the surface layers. This method has since been widely diffused around the world by Nakamura [1989]. Since 1989, because of its low-cost and its fast deployment, the use of the H/V method has become widespread, mainly with the objective of detecting the sedimentary zones that could amplify seismic ground motion. The validation of the H/V spectral ratio using noise has been since confirmed both experimentally [Lermo and Chávez-García, 1993; Field and Jacob, 1995; Guéguen et al., 2000; Lebrun et al., 2001] and from theoretical and numerical studies [Field and Jacob, 1993; Lachet and Bard, 1994; Cornou et al., 2004; Bonnefoy-Claudet, 2004]. In the case of a stratified soil profile composed of a soft layer at the top of a stiffer layer, the 1D amplified frequency f_0 may be estimated according to the equation $f_0=Vs/4Hs$, where Hs is the thickness and Vs the shear wave velocity of the topmost layer, respectively and when the S-wave contrast is sufficiently large [Bonnefoy-Claudet, 2004]. As outlined by the equation linking f_0 to Hs, knowing the shear wave velocity Vs of the upper layer is fundamental to deduce the thickness of this layer. This information can be derived from S-wave refraction or surface wave analyses. Nevertheless, the simple relation linking fundamental frequency, shear wave velocity and depth is valid according to a 1D model assumption that is not the geometry

of most valleys. For example, while Bard & Bouchon [1985] discussed the 2D model shapes of a theoretical valley, Steimen et al. [2003] and Roten et al. [2004] recently showed experimentally the strong 2D effect of valley shape on the resonance frequency deduced from ambient seismic noise.

The shear wave velocity profile can also be obtained from seismic noise measurements recorded by an array of seismometers. This configuration allows to define the dispersion curve of the Rayleigh-wave phase velocity [for example, Tokimatsu, 1997; Satoh et al., 2001; Scherbaum et al., 2003].

In the following, all dispersion curves deduced from active surface wave or from seismic noise network analyses, were computed using the conventional semblance-based frequency-wavenumber method [Lacoss et al., 1969; Kvaerna and Ringdahl, 1986; Ohrnberger, 2001], which provides a semblance map of the velocity (or slowness) and frequency of the waves travelling with the highest energy. The maximum of each semblance map has been picked.

The obtained dispersions curves were then inverted to obtain the S-wave vertical velocity profile (and eventually VP). For this, we used a neighbourhood algorithm inversion method where the computation time has been optimized [Wathelet et al., 2004]. The method is a stochastic direct search method for finding models of acceptable data fit within a multidimensional parameter space [Sambridge, 1999a & 1999b]. Four parameters were investigated, *ie.* thickness, density, P-wave velocities and (above all) S-wave velocities of each layer. Thousands of direct models were tested and only those exhibiting lower RMS errors were kept. It should be noted that to reduce the number of models, the H/V resonance frequency of the central station was added as *a priori* information during the inversion process.

INVESTIGATION OF THE SUPER-SAUZE MUDSLIDE

Geological, geomorphological and geotechnical setting of the mudslide

The Super-Sauze mudslide (Ubaye valley) is one of the persistently active landslide (since the 1970's) occurring in black marls [Malet and Maquaire, 2003]. Its geological environment is very complex and is the consequence of the geological history of this alpine zone characterized by an overthrust of allochtonous sandstone and limestone formations over the autochtonous black marl bedrock. From the highest to the lowest elevations, the geological levels comprise: (1) the calcareous Klippe of Lan which overhangs the mudslide, (2) the moraine deposited by the Ubaye glacier during the Quaternary age, (3) the autochtonous bedrock consisting of Callovo-Oxfordian black marls with a grey clayey schist facies, very finely laminated and highly tectonized.

It is a clayey flow-like landslide characterized by a complex vertical structure associating a slip surface and a viscoplastic plug. Multidisciplinary observations (geology, geomorphology, geotechnics, hydrology) carried out since 1991 [Weber and Hermann, 2000; Flageollet et al., 2004] provide numerous information about its geology and geometry. The mudslide material consists of a silty-sand matrix mixed with moraine debris. It extents over an horizontal distance of 850 m and occurs between an elevation of 2105 m at the crown and 1740 m at the toe with an average 25° slope. Its total volume is estimated at 750,000 m^3 and velocities range from 0.01 to 0.4 $m.day^{-1}$ [Malet and Maquaire, 2003]. A detailed morphological description of the mudslide since its genesis can be found in Weber and Herrmann [2000]. The bedrock topography corresponds in the upper part to a succession of more or less parallel crests and gullies and in the medium and lower parts to a narrow and deeply incised channel. Consequently its thickness is highly variable and varies between 0 and about 20 m. This

geometrical scheme plays an essential role in the dynamics of the landslide by delimiting preferential water and material pathways and creating sections with differing kinematical, mechanical and hydrological characteristics. Its geotechnical structure consists in two superimposed units [Flageollet et al., 2004; Malet and Maquaire, 2003]. The topmost unit, 5 to 9 m thick, is a very wet muddy formation, whereas the lowermost unit, with a maximum thickness of 10 m, is a stiff compact, relatively impervious and apparently stable formation. The hillslopes delimitating the lateral extension of the mudslide are characterized by moraine deposits, 3 to 15m thick, especially on the eastern flank.

Electrical Tomographies

Six electrical tomographies were carried out on the mudslide allowing a pseudo-3D view of its internal structure (fig. 2, white lines). The tomographies were acquired using a Wenner configuration chosen for its high signal to noise ratio property and its sensitivity to horizontal contrasts, although the configuration is not adapted to precisely image lateral contrasts [Dahlin & Zhou, 2004]. Transverse profiles A1, A2 and A3 were acquired using 64 electrodes spaced every 4 m in the upper part of the mudslide. Transverse profiles C1 (80 electrodes, 4 m spacing) and C2 (48 electrodes, 5 m spacing) were acquired in the medium part of the mudslide. Finally, the longitudinal CA profile (64 electrodes, 5 m spacing) was acquired between transects C1 and A1. The raw data were inverted separately in 2D using the RES2DINV inversion software [Loke and Barker, 1996], considering an L2-norm for optimisation. Derived resistivity images present RMS errors lower than 3% after 5 iterations.

These electrical images (fig. 3) show a clear contrast between the mudslide material with low resistivity values (less than 90 Ω.m) and the stable black marls bedrock with higher

resistivity values (more than 150 Ω.m). These resistivity values are comparable to those obtained by Schmutz et al. [2000] from joint-inversion of VES and TDEM data, who found a resistivity range of 2 to 50 Ω.m for the active unit and more than 400 Ω.m for the substratum. The increase of resistivity values with depth observed in the mudslide material can be explained by a decrease of the hydraulic conductivity with depth due to both the presence of water-saturated cracks in the topmost layer and compaction of the lowermost layer. On the eastern part of profiles C1 and C2, higher resistivity values (more than 700 Ω.m) are observed; they correspond to stable hillslopes formed of moraine deposits. These electrical tomographies correctly image the transverse and to a lesser degree the longitudinal thickness changes of the mudslide, underlying its complex bedrock topography.

In the medium part of the mudslide, the electrical images indicate a total thickness ranging from 24 m to less than 5 m along the C1 and C2 profiles; this geometry is consistent with the depth variations proposed by Malet & Maquaire [2003] for this section on the basis of geotechnical tests. In the upper part of the mudslide, a more or less constant thickness of 18 m is found along the A1 profile, while the A2 and A3 profiles indicate strong lateral changes due to the presence of in-situ buried bedrock crests. These profiles point out a deeper bedrock (more than 30 m) than in the medium part. Although geotechnical in this part of the mudslide are more scarce, the resistivity variations seem in accordance with the combined geomorphological-geotechnical interpretation suggested by Malet [2003]. As these tomographies were acquired in the autumn season, the surface formations present larger resistivity values probably due to dryer hydrological conditions. Finally, the longitudinal electrical image indicates smooth vertical variations, with a maximum depth reaching 18 m at the intersection with the C1 profile.

To summarize, the tomography profiles provided valuable and continuous information about the pseudo-3D geometry of the mudslide. These data will be used in zones lacking of geotechnical measurements for interpreting seismic noise interpretation.

H/V method

Three H/V seismic noise profiles were performed on the mudslide (fig. 2). Two of them (C and B) were acquired in the transverse direction, along the C and B geotechnical cross-sections, considering 15 m and 10 m spacing between each seismometer, respectively. A longitudinal profile (CA) was acquired between the A and C geotechnical cross-sections, with a 10 m spacing. In our experiments, we used six 3D Lennartz sensors (5 seconds), which gave flat responses in the [0.2-50 Hz] frequency range. They were connected to a CityShark^{TM} II acquisition system developed for noise measurement [Chatelain et al., 2000]. Ambient vibration data were sampled at 200 Hz and recorded for 30 minutes. Among these 30 minutes, a maximum of short time windows (about 40 seconds) are selected through an anti-trigger process in order to select the more stable signal of noise ratio, *ie.* without transient high-frequency waves. Finally, Fast Fourier Transforms were processed for the three components and the spectral ratio was computed for each horizontal component (*ie.*, *H1/V* and *H2/V*) as well as the quadratic average of the spectral ratio (*H/V*). Interesting recommendations for acquisition and processing tools dedicated to H/V measurements can be found in the conclusions of the SESAME European Research Project [2005]. To investigate complex and irregular structures, Uebayashi [2003] suggested orientating one component of the seismometer parallel to the structure variations because the frequency peak amplitude is sensitive to the orientation of the horizontal component. Therefore, on profiles CA and C the

spectral ratio was computed using the E-W component, as the most important change is expected to occur along the longitudinal axis of the mudslide. On profile B, the spectral ratio was computed using the N-S components the geotechnical investigations indicate large lateral variations in the bedrock depth.

Figures 4a, 4b and 4c present H/V spectral ratios calculated in the [0.2-20 Hz] frequency range for the 3 profiles. The frequency is represented on the vertical axis, point numbers are indicated on the horizontal axis and colours represent the Naperian logarithm of the horizontal to vertical spectral ratio. The black dot points correspond to the picked frequency peaks and the white dot lines represent the intersections with other profiles. Figure 4d maps the spatial variation of the picked frequency (colour scale) including those concerning the seismic noise network.

On profile CA, a clearly distinguishable dominant frequency can be easily picked; this dominant frequency varies smoothly along the profile. For some points, higher frequencies exhibiting higher H/V amplitudes could have been wrongly picked (*eg.*, like for point 7, with two major frequencies around 10 Hz and 15 Hz; but also lower frequencies at some points). Even if the structure along this profile is 3D, the dominant frequency varies continuously and this feature can be explained by the smooth variations of the thickness along the profile, and by a well-adapted spatial sampling (10 m). In this case, no 3D effects significantly disturb both data acquisition and data processing, implying that surface waves propagation can be considered as 1D [Bonnefoy-Claudet, 2004]. On the contrary, it is clear that problems arise for profile B, where different resonance frequencies can be picked for a single point measurement, probably generated by different layers. In this case of large lateral thickness variations at a small-scale, the chosen spatial sampling (every 10 m) is too large to identify

continuous variations of the suitable frequency. A blind frequency picking performed considering the maximum H/V amplitudes resulted in too large heterogeneities. Consequently, we decided to pick two frequencies on some points, and propose a non-unique interpretation (fig. 5), considering the presence of several layers. To overcome this problem, a more adapted sampling scheme may improve the interpretation. In our case, the low-frequencies appearing mainly on the flanks of the mudslide must be related to a deeper interface (probably linked with the presence of former coarse mudslide), which was identified on electrical images. Other points (11, for example), exhibited unexplained low frequency amplification, probably due to acquisition problems linked with coupling effects or local subsurface heterogeneities, disturbing the surface wave propagation. Profile C1 is a mix between the two previous examples. The observed variations are smoother, and the pickings appear realistic (fig. 5) except in the eastern part of the profile (from tests 1 to 5, where tests 1 to 3 are located outside of the mudslide). Again, this ambiguity must come from the presence of former coarse mudslide. Finally, the seismic noise measurements recorded for the network experiment (fig. 4d) exhibit consistent frequencies with those deduced from the profiles, underlying a smooth geometry in this part of the mudslide.

Figure 5 presents the interpretation of the picked frequencies in term of thickness (red points). The thickness was computed by using the formula $f_0=Vs/4Hs$ and considering a constant shear velocity Vs = 260 $m.s^{-1}$ in the mudslide. This velocity was deduced from the surface waves and from the seismic noise network analyses (fig. 6, fig. 7). The presence of two peaks in some H/V ratios (fig. 4b, fig. 4c) resulted in two possible interpretations, although lower frequencies are expected to be due to the presence of deeper interfaces (former coarse mudslide), acquisition problems or local heterogeneity. The bedrock geometry was deduced from geotechnical data when available (black points), photogrammetric stereo-

restitution of the topography before and after the mudslide [Weber and Herrman, 2000], and H/V interpretation. The surface topography changes between 1996 (when the geotechnical investigation was carried out) and 2005 (when the geophysical acquisition was carried out) were taken into account. Finally, the blue dashed line corresponds to the interpretation of electrical tomographies (fig. 3). The limit was adjusted using geotechnical measurements. These results show that the interpretation of the picked frequency in term of thickness is particularly consistent with other measurements, even if the structure is 3D. However, it is clear that when H/V spectral ratios exhibit more than one peak in the interesting frequency range, interpretation is more doubtful and a spatial over-sampling is needed. Variability of the mudslide shear wave velocity can also explain the small differences between the known geometrical model and the estimated thickness. It should be noted that electrical interpretation is well consistent with the deduced interface on the bottom of the CA profile, but less on the C profile. These differences must be due to the lack of precision of smooth electrical tomography, particularly when lateral variability is present for the used Wenner configuration.

Seismic noise network

An array noise experiment was performed in the middle part of the C cross-section (fig. 2), consisting of three circle arrays (radius of 10, 25 and 50 m) each composed of 6 seismic stations. To compare the dispersion curve derived from these measurements, a longitudinal active seismic line was recorded along the CA profile (fig. 2) using 24 4.5 Hz-vertical geophones placed every 10 m.

Figure 6e displays the dispersion curve computed from the passive seismic noise arrays and associated error) and the semblance map of the energy of the active surface waves. It must be underlined that only two seismic noise arrays (radius of 10 and 25 m) were used (transition frequency around 7 Hz on the dispersion curve), the larger one (50 m radius) presenting no dispersion effect (certainly due to 3D effects for these wavelengths). These dispersion curves are well consistent and display the same variations except for low frequencies. This demonstrates that the seismic noise measurements are mainly composed of surface waves which is one of the major assumptions for seismic noise interpretation (with the 1D hypothesis).

The inversion results are displayed on figures 6c and 6d for the seismic noise and figure 6a and 6b for the active surface waves. During the inversion process, the H/V peak was added as a priori information only for the seismic noise inversion. On figures 6b and 6d, the experimental inverted dispersion curve computed from real data are superimposed to the models derived after inversion, the low RMS errors being presented in red. For both inversions, best models show S-waves velocity ranging between 260 and 300 $m.s^{-1}$ for the topmost layer. They also show a well-defined thickness between 19-22 m for the noise and not well defined thickness between 16 and 20 m for the surface waves. All these results are consistent with other data acquired on this smooth area, which was densely imaged from electrical measurements and H/V data. It is noticeable that both results also showed thin contrasts inside the mudslide, which could be related to the observed superimposed units discussed before. The shear wave velocity of the bedrock is not so well retrieved. It varies between 600-700 $m.s^{-1}$ for the surface waves and between 1100-1300 $m.s^{-1}$ for the seismic noise. Considering the large uncertainty on the dispersion curve of the seismic noise at low frequencies, it may be reasonable to keep the velocity deduced from surface waves.

To summarize, combined seismic noise arrays were able (1) to derive consistent surface wave dispersion curves compared to those provided from active surface wave analysis, and (2) to propose inversion models constrained with H/V information which retrieved precisely S-wave velocity and thickness of the mudslide. With lower frequencies (network radius >20m), thickness and S-wave velocity of the bedrock may have been more precisely investigated.

INVESTIGATION OF THE SAINT-GUILLAUME TRANSLATIONAL LANDSLIDE

Geological, geomorphological and geotechnical setting of the translational landslide

The Saint-Guillaume landslide is located in the Trièves basin (fig 1) where many clayey landslides have occurred in the past in the so-called varved clays; these clays are finely laminated glacio-lacustrine deposits dating from the Pleistocene (Wurmenien) period [Antoine et al., 1981; van Asch et al., 1996]. The observed landslides present slip surfaces at different depths [Antoine et al., 1981; Nieuvenhuis, 1991] from almost shallow ones (4 to 8 m) to more deeper ones (20 to 40 m).

The investigated landslide is a slow (1-5 $cm.year^{-1}$) translational landslide affecting the small village of Saint-Guillaume. The geological basement is composed of Oxfordian marly limestone covered with 40 to 50 m of varved clays. The landslide is limited to the South by a limestone cliff overhanging a scree-covered hillslope (fig. 7). A umbilical zone of limestone is also visible to the East sub-dividing the clay formation in two parts. To the North the landslide is limited by the Gresse torrent which has incised a narrow channel in the varved

clays. In the Western part of the landslide a geomorphological survey (geomorphological map, topographic control points) and a geotechnical investigation (three inclinometers, one piezometer) have been carried out in the late nineties. The boreholes have pointed out the existence of an interface between the uppermost varved clay and the marly limestone bedrock at 38.5 m, 61.7 m and 33.1 m depths at I1, I3 and I4 boreholes respectively (fig. 7). The inclinometers detected sometimes several slip surfaces inside the clay formation; the main slip surfaces were located at 34.5 m, 37.0 m, and 27.0 m depth, respectively. This monitoring system has been complemented since 2003 by geophysical investigations. Those are described in Garambois et al. (submitted). As a consequence, only a sum up of the main characteristics of the landslide is developed hereafter. As for the Super-Sauze mudslide, seismic noise measurements (H/V and seismic noise network) were tested (fig. 7). The comparison with Super-Sauze is interesting because Saint-Guillaume presents smoother bedrock geometry and thinner S-wave contrast.

H/V method

The H/V profile was carried out along an East-West direction perpendicular to the main displacement of the landslide. Measurements were made every 20 m, including in the village and on the marly limestone bedrock arising at the surface (tests 70 to 80). Figure 8a highlights the presence of two resonance frequencies, respectively around 1.3 Hz and 2 Hz. They are joined between tests 55 and 76 (high single frequency) and on the edges of the profiles (low single frequency). When the bedrock arises to the ground surface, both frequencies vanished. Considering S-wave refraction [Garambois et al., 2006, submitted] and surface wave analysis (fig. 9), the S-wave velocity of the upper layer is around 260 $m.s^{-1}$. We consequently interpreted the higher frequency in term of thickness with this velocity (fig. 8b). The interface

lies between 0 (where the bedrock reaches the surface) and 50 m. Black dots located on test 32 represent the known slip surface and bedrock depth in the I3 inclinometer. The lower frequency is more difficult to interpret. As it vanishes when bedrock reaches surface, it may correspond to the signature of the clay/marly limestone interface located at 61 m at inclinometer I3 (fig. 8b). For the frequency to depth conversion, we used a velocity profile as a function of depth, which was deduced from S-wave refractions analysis and surface waves analysis (fig. 9). Both showed that the undisturbed clays exhibit a velocity around 550 m/s. Using an equivalent velocity ($Vs_{equivalent} = (Vs_{disturbed\ clays} * H_{disturbed\ clays} + Vs_{undisturbed\ clays} * H_{undisturbed\ clays})/(H_{disturbed\ clays} + H_{undisturbed\ clays})$), the low frequency was picked and converted into depth, allowing to obtain an image of the bedrock geometry. The derived curve is relatively well consistent with the I3 deduced bedrock depth and remarkably with an electrical tomography image reaching 80 m depth [Garambois et al., 2006, submitted]. All the results suggest that the landslide develop first at the clay/bedrock interface when bedrock reaches the surface, and then within the clay layer (as confirmed by inclinometer monitoring). Compared to the Super-Sauze mudslide, frequency picking was easier certainly because the structures are less 3D and present less heterogeneity.

Seismic noise network

Seismic noise arrays, performed around inclinometer I3, are composed of three arrays, with radius of 20, 40 and 60 m (fig. 7). Again, this investigation was combined to an active seismic experiment using 24 4.5 Hz-vertical geophones. All data were processed in the same way than in the Super-Sauze investigation. Figure 9 presents the results derived from both passive and active seismic surveys. The frequency range of the dispersion curves largely differs depending on the method. Indeed, the passive method provided useful information in

the [2.5-6.5 Hz] frequency range and the active method in the [4-12 Hz] frequency range. In the [4-6.5 Hz] frequency range, both dispersion curves are remarkably consistent, as displayed on figure 9c. This observation shows that the larger part of the energy contained in the seismic noise is made of surface waves. The inversion process was performed using the H/V constrain for the passive network.

Both best models (low RMS) are consistent with the geotechnical and geophysical data. The S-wave velocity of the topmost layer is well constrained in both experiments, ranging from 260 to 280 $m.s^{-1}$, although seismic noise dispersion curve exhibited few high frequencies. It corresponds to the unstable clayey zone highly affected by deformation. Its thickness is also relatively well-defined, ranging from 31 to 34 m for the passive seismic noise method and from 28 to 30 m thick for the active method. The difference may arise from the 3D homogenisation property of the array, which integrates the information on a larger zone and includes variability in landslide thickness. Moreover, it must be noted that the surface wave acquisition was performed on the N-W edge of the array.

As discussed before, S-wave velocity varies around 550 $m.s^{-1}$ ($Vp=1800\ m.s^{-1}$) in the stable part of clays, and reaches more than 800 $m.s^{-1}$ ($Vp > 2500\ m.s^{-1}$) in the marly limestone bedrock. Figure 9 clearly outlines that both methods found best models displaying S-wave velocity around 600 m/s for the second layer (the stable clays). However, they were unable to detect and characterize the bedrock interface, although there is a large increase of Rayleigh velocity at low frequencies for the seismic noise network (but with a large uncertainty).

CONCLUSIONS

Two seismic noise experiments were performed on two landslides presenting different characteristics: (1) a mudslide characterized by abrupt 3D variations in the bedrock geometry

and large S-wave velocity contrasts, and (2) a translational landslide where the slip surface geometry as well as the S-wave contrasts are smoother. H/V measurements showed their efficiency in characterizing the contact between the stable and unstable material for both landslides, as well as the bedrock interface for the translational landslide. Difficulties arise on the mudslide, as multiple resonance frequencies appeared. Some of them may be due to deeper interfaces, heterogeneities or bad coupling effects during the acquisition. To increase interpretation confidence, an adapted spatial sampling must be adapted to the 3D structure effect.

Inversions of dispersion curves obtained from seismic noise arrays on both sites were compared to geotechnical data, as well as to results provided by active surface wave investigations. First, a clear correlation between active and seismic dispersion curves indicated that in both cases seismic noise was mainly composed of surfaces waves. Second, large arrays are not always efficient. For the Super-Sauze mudslide, the larger array enabled to record consistent dispersive waves at low frequencies.

In soft-rock landslides, slip surfaces appear to generate large S-wave velocity contrasts that seismic noise methods are able to detect and characterize properly. Consequently, combined to theoretical studies, seismic noise methods may be of high interest to identify and map slip surfaces in 3D.

AKNOWLEDGMENTS

This work was supported by grants from the French Ministry of Research within the ACI project SAMOA 'Surveillance et Auscultation de MOuvements gravitaires Alpins' (Coordinators: C. Delacourt, O. Maquaire and D. Amitrano) and the ACI project GACH2C 'Glissements Alpins à Contrôle Hydrologique et Changement Climatique' (Coordinators: O. Maquaire and J.-P. Malet). The investigation carried out at Saint-Guillaume was supported by grants from the Conseil Général de l'Isère within a 'Pôle Grenoblois des Risques Naturels' project.

We express our gratitude to the RTM38 and particularly to Mrs. Catherine Moulin for providing geotechnical data on the Saint-Guillaume landslide. We also thank all colleagues who helped us during the field investigation, as well as the people from the city office of Saint-Guillaume.

REFERENCES

ANTOINE P., GIRAUD A. & MONJUVENT G. (1981) - Les argiles litées du Trièves (Isère), conditions de glissement de terrain et exemples de propriétés géotechniques - *Bulletin de la Société Géologique de France*, **23**, 117-127.

ASTEN M. W. (2004). - Passive seismic methods using the microtremor wave field for engineering and earthquake site zonationEds., *74th SEG Annual Meeting*. Denver, USA. 10-15 October 2004.

BARD, P.-Y., & M. BOUCHON (1985) - The two-dimensional resonance of sediment-filled valleys - *Bull. seism. Soc. Am.*, 75, 519-541.

BONNEFOY-CLAUDET S. (2004) - Nature du bruit de fond sismique : implications pour les études des effets de site. - PhD thesis, Grenoble University, France, 241 p.

CHATELAIN J. L., GUÉGUEN P., GUILLIER B., FRECHET J., BONDOUX F., SARRAULT J., SULPICE P. & NEUVILLE J. M. (2000) - CityShark: A user-friendly instrument dedicated to ambient noise (microtremor) recording for site and building response studies. - *Seismological Research Letters*, **71(6)**, 698-703.

COMMEND S., GEISER F. & TACHER L. (2004). - 3D numerical modelling of a landslide in Switzerland,, Proceedings of *NUMOGIX*, Ottawa, 2004.

CORNOU C., KRISTEK J., OHRNBERGER M., DIGUILIO G., SCHISSELE E., GUILLIER B., BONNEFOY-CLAUDET S., WATHELET M., FAEH D., BARD P.-Y. &

MOCZO P. (2004). - Simulation of seismic ambient vibrations – II: H/V and array techniques for real sites Eds., *13th World Conf. Earth. Engng.* Vancouver, BC Canada, 1130.

DAHLIN, T & B. ZHOU (2004) - A Numerical Comparison of 2D Resistivity Imaging with Ten Electrode Arrays - *Geophysical Prospecting*, 52, 379-398.

FIELD E. & JACOB K. (1993) - The theoretical response of sedimentary layers to ambient seismic noise - *Geophysical Research Letters*, **20**, 2925-2928.

FIELD E. & JACOB K. (1995) - A comparison and test of various site-response estimation techniques including three are not reference-site dependent. - *Bulletin of the Seismological Society of America*, **85**, 1127-1143.

FLAGEOLLET J.-C., MALET J.-P., SCHMUTZ M. & MAQUAIRE O. (2004). - Integrated investigations on landslides: example of the Super-Sauze earthflow. In CASALE R. & MARGOTTINI C., Eds., *Natural Disaster and Sustainable Development*. Springer - Verlag, Berlin., 213-238.

GALLIPOLI, M., V. LAPENNA, P. LORENZO, M. MUCCIARELLI, A. PERRONE, S. PISCITELLI, AND F. SDAO (2000) - Comparison of geological and geophysical prospecting techniques in the study of a landslide in southern Italy - *European Journal of Environmental and Engineering Geophysics*, **4**, 117–128.

GARAMBOIS S., GUÉGUEN P. & CRAVOISIER S. (2006) - A comparative study between geophysical and seismic noise measurements for clayey soil landslides characterization - *Canadian Geotechnical Journal*, submitted.

GIRAUD A., ANTOINE P., VAN ASCH T. W. J. & NIEUWENHUIS J. D. (1991) - Geotechnical problems caused by glaciolacustrine clays in the French Alps - *Engineering Geology*, **31**, 185-195.

GUÉGUEN, P., J.-L. CHATELAIN, B. GUILLIER & H. YEPES (2000) - An indication of the soil topmost layer response in Quito (Ecuador) using H/V spectral ratio - *Soil Dynamics and Earthquake Engineering*, 19, 127-133.

ISRAIL M. & PACHAURI A. K. (2003) - Geophysical characterisation of landslide site in the Himalayan foothill region - *Journal of Asian Earth Sciences*, **22**, 253-263.

JONGMANS D. & GARAMBOIS S. (2006) - Surface geophysical and monitoring of landslides: a review - *Bull. Soc. Géol. France*, submitted.

KVAERNA T. & RINGDAHL F. (1986). - Stability of various f-k estimation techniques. -, Report 1-86/87, NORSAR Scientific Report, Kjeller, Norway.

LACHET C. & BARD P. (1994) - Numerical and theorical investigations on the possibilities and limitations of the "Nakamura's" technique. - *Journal of Physics of the Earth (Japan)*,

LACOSS R. T., KELLY E. J. & TOKSÖZ M. N. (1969) - Estimation of seismic noise structure using arrays - *Geophysics*, **34**, 21-38.

LEBRUN B., HATZFELD D. & BARD P.-Y. (2001) - A site effect study in urban area: experimental results in Grenoble (France) - *Pageoph.*, **158**, 2543-2557.

LERMO J. & CHÁVEZ-GARCÍA F. J. (1993) - Site effect evaluation using spectral ratios with only one station - *Bulletin of the Seismological Society of America*, **83**, 1574-1594.

LOKE M. H. & BARKER R. D. (1996) - Rapid least-squares inversion of apparent resistivity pseudosections by a quasi-Newton method. - *Geophysical Prospecting*, **44**, 131-152.

MALET J.-P. (2003) - Les 'glissements de type écoulement' dans les marnes noires des Alpes du Sud. Morphologie, fonctionnement et modélisation hydro-mécanique. - *Institut de Physique du Globe*, 331 p. - Thèse, Strasbourg, 2003.

MALET J.-P. & MAQUAIRE O. (2003) - Black marl earthflows mobility and long-term seasonal dynamic in southeastern France. In PICARELLI L., Eds., *International Conference*

on Fast Slope Movements: Prediction and Prevention for Risk Mitigation. Bologna. Patron Editore, 333-340.

MALET J.-P., VAN ASCH T. W. J., VAN BEEK L. P. H. & MAQUAIRE O. (2005) - Forecasting the behaviour of complex landslides with a spatially distributed hydrological model - *Natural Hazards and Earth System Sciences*, **5**, 71-85.

MAQUAIRE O., FLAGEOLLET J.-C., MALET J.-P., SCHMUTZ M., WEBER D., KLOTZ S., ALBOUY Y., DESCLOÎTRES M., DIETRICH M., GUÉRIN R. & SCHOTT J.-J. (2001) - Une approche multidisciplinaire pour la connaissance d'un glissement coulée dans les marnes noires du Callovien-Oxfordien (Super-Sauze, Alpes de Haute Provence, France) - *Revue Française de Géotechnique*, **95/96**, 15-31.

McCANN D. M. & FORSTER A. (1990) - Reconnaissance geophysical methods in landslide investigations - *Engineering Geology*, **29**, 59-78.

MERIC O., GARAMBOIS S., JONGMANS D., WATHELET M., CHATELAIN J. L. & VENGEON J. M. (2005) - Application of geophysical methods for the investigation of the large gravitational mass movement of Séchilienne, France - *Canadian Geotechnical Journal*, **42**, 1105-1115.

NAKAMURA Y. (1989) - A method for dynamic characteristics estimation of subsurface using microtremor on groung surface - *QR of RTRI*, **30**, 25-33.

NIEUWENHUIS J. D. (1991). - The lifetime of a landslide: investigation in the French Alps. - *FRANCIS T.*, London, p. 160

NOGOSHI, M., & T. IGARASHI, (1971) - On the amplitude characteristics of microtremor (part 2) - *Journal of Seismological Society of Japan*, 24, 26-40.

ROTEN, D., C. CORNOU, S. STEIMEN, D. FAEH & D. GIARDINI (2004) - 2D resonances in Alpine valleys identified from ambient vibration wavefield, *in Proc. 13th World Conf. on Earthq. Engng.*, Vancouver, Canada BC, August 2004.

SAMBRIDGE M. (1999b) - Geophysical inversion with a neighbourhood algorithm-II. Apprising the ensemble - *Geophys. J. Int.*, **138**, 727-746.

SAMBRIDGE M. (1999a) - Geophysical inversion with a neighbourhood algorithm- I. Searching a parameter space - *Geophys. J. Int.*, **138**, 479-494.

SATOH T., KAWASE H. & MATSUSHIMA S. (2001) - Estimation of S-Wave Velocity Structures in and around the Sendai Basin, Japan, Using Array Records of Microtremors - *Bulletin of the Seismological Society of America*, **91**, 206-218.

SCHERBAUM F., HINZEN K.-G. & OHRNBERGER M. (2003) - Determination of shallow shear wave velocity profiles in the Cologne/Germany area using ambient vibrations. - *Geophysical Journal International*, **152**, 597-612.

SCHMUTZ M., ALBOUY Y., GUÉRIN R., MAQUAIRE O., VASSAL J., SCHOTT J.-J. & DESCLOÎTRES M. (2000) - Joint electrical and time domain electromagnetism (TDEM) data inversion applied to the Super Sauze earthflow (France) - *Surveys in Geophysics*, **21**, 371-390.

SESAME EUROPEAN RESEARCH PROJECT (2005) - Guidelines for the implementation of the H/V spectral ratio technique on ambient vibrations measurements, processing and interpretation, report, http://sesame-fp5.obs.ujf-grenoble.fr/SES_TechnicalDoc.htm, 62 p.

STEIMEN, S., D. FÄH, F. KIND, C. SCHMID & D. GIARDINI (2003) - Identifying 2-D Resonance in Microtremor Wave Fields - *Bull. Seism. Soc. Am.*, 93, 583 – 599.

TACHER L., BONNARD C., LALOUI L. & PARRIAUX A. (2005) - Modelling the behaviour of large landslide with respect to hydrogeological and geomechanical parameter heterogeneity - *Landslides*, **2**, 3-14.

TOKIMATSU K. (1997). - Geotechnical site characterization using surface waves. In ISHIHARA, Eds., *Earthquake Geotechnical Engineering*. Rotterdam. Balkema, 1333-1368.

UEBAYASHI H. (2003) - Extrapolation of Irregular Subsurface Structures Using the Horizontal-to-Vertical Spectral Ratio of Long-Period Microtremors - *Bulletin of the Seismological Society of America*, **93**, 570-582.

VAN ASCH T. W. J., HENDRICKS M., HESSEL R. & RAPPANGE F. E. (1996) - Hydrological triggering conditions of landslides in varved clays in the French Alps - *Engineering Geology*, **42**, 239-251.

WATHELET M., JONGMANS D. & OHRNBERGER M. (2004) - Surface wave inversion using a direct search algorithm and its application to ambient vibration measurements - *Near Surface Geophysics*, **2**, 221-231.

WEBER D. & HERRMANN A. (2000) - Contribution de la photogrammétrie numérique à l'étude spatio-temporelle de versants instables : l'exemple du glissement de terrain de Super-Sauze (Alpes-de-Haute-Provence, France) - *Bull. Soc. Géol. France*, **6**, 637-648.

YAMAMOTO H. (1998). - An experiment for estimating S-wave velocity structure from phase velocities of Love and Rayleigh waves in microtremors.Eds., *Second International Symposium on the Effect ofSurface Geology on Seismic Motion*. Yokohama, Japan. 1-3 December 1998. Balkerna, A.A./Rotterdam/Brookfield, **2**, 705-710.

FIGURE CAPTIONS

Figure 1: Locations of the two test sites: translational landslide of Saint-Guillaume and mudslide of Super-Sauze, South French Alps.

Figure 2: 3D topography image of the Super-Sauze mudslide and locations of the geophysical and seismic noise measurements. White lines: electrical tomography; black dots: seismic noise measurements (H/V); black triangles: seismic noise network.

Figure 3: Electrical tomography images derived after inversion of data acquired using a Wenner acquisition at the Super-Sauze mudslide.

Figure 4: H/V and seismic noise network results obtained at the Super-Sauze mudslide along the B profile (a), the C profile (b) and the CA longitudinal profile (c). The picked frequency is displayed in colour (d), including H/V measurements acquired during the seismic noise network experiment.

Figure 5: Interpretation of H/V picked frequencies of the Super-Sauze mudslide considering a mean S-wave velocity of 260 $m.s^{-1}$. It was compared to geotechnical and electrical data. The interface was drawn considering all the results, except electrical tomography.

Figure 6: Inversion results of the dispersion curve obtained from the seismic noise network and the surface wave measurements at the Super-Sauze mudslide. Vs models as a function of depth and of RMS error (colour scale) for the SW (a) and the seismic noise (c). Superimposition of the dispersion curve with the derived models for the SW (b) and the seismic noise (d). (e) Superimposition of the seismic noise dispersion curve and the semblance map of surface waves.

Figure 7: Aerial photograph of the Saint-Guillaume landslide, including locations of the three inclinometers, the seismic noise measurements and a schematic view of the geology (a). Enlargement of the seismic noise investigation zone (right).

Figure 8: H/V results obtained at Saint-Guillaume landslide (a) and interpretation of the picked frequencies in term of sliding surface and bedrock geometries. The black dot represents depths deduced from the inclinometer and borehole measurements (b).

Figure 9: Inversion results of the dispersion curve obtained from the seismic noise network and the surface wave measurements at the Saint-Guillaume landslide. Vs models as a function of depth and of RMS error (colour scale) for the SW (a) and the seismic noise (c). Superimposition of the dispersion curve with the derived models for the SW (b) and the seismic noise (d). (e) Superimposition of the seismic noise dispersion curve and the semblance map of surface waves.

LEGENDE DES FIGURES

Figure 1: Localisation des deux sites tests : Le glissement translationel de Saint-Guillaume et le glissement-coulée de Super Sauze, Alpes du sud de la France.

Figure 2: Image 3D de la topographie du glissement-coulée de Super-Sauze et positionnement des mesures géophysiques et de bruit de fond sismique. Lignes blanches : tomographies électrique ; points noirs : points de mesures du bruit de fond sismique (H/V) ; triangles noirs : capteurs du bruit de fond réseau.

Figure 3: Image de tomographies électrique déduites après inversion de données acquis en mode Wenner sur le glissement-coulée de Super-Sauze.

Figure 4: Résultats des mesures H/V obtenues sur le glissement-coulée de Super-Sauze le long du profil B (a), du profil C (b) et du profil longitudinal CA (c). Le pic de fréquence est représenté par un code de couleur (d), incluant les mesures H/V obtenues lors de l'acquisition du bruit de fond réseau.

Figure 5: Interprétation des fréquences pointées des mesures H/V sur le glissement-coulée de Super-Sauze considérant une vitesse de 260 $m.s^{-1}$. Ces interprétations sont comparées aux données géotechniques et électriques. L'interface a été dessinée considérant tous les résultats, exceptés ceux de la tomographie électrique.

Figure 6: Résultats de l'inversion de la courbe de dispersion du réseau de bruit de fond sismique et des mesures d'onde de surface sur le glissement-coulée de Super-Sauze. Modèles de Vs en fonction de la profondeur et de l'erreur (échelle de couleur) pour les ondes de surface (a) et pour le bruit sismique (c). Surimposition de la courbe de dispersion avec les modèles dérivée des ondes de surface (b) et du bruit de fond sismique (d). (e) Surimposition de la courbe de dispersion issue du réseau de bruit de fond sismique et de la carte de semblance des ondes de surface.

Figure 7: Photographie aérienne du glissement de Saint-Guillaume avec la localisation des trois inclinomètres, des mesures de bruit de fond et une vue schématique de la géologie (a). Agrandissement de la zone d'investigation pour le réseau de bruit de fond sismique (b).

Figure 8: Résultats du H/V mesuré sur le glissement de Saint-Guillaume (a) et interprétation des fréquences pointées en termes de géométrie surface de glissement et de substratum. Les points noirs représentent les profondeurs déduites de l'inclinomètre I3 et des mesures en sondage (b).

Figure 9: Résultats de l'inversion de la courbe de dispersion du réseau de bruit de fond sismique et des mesures d'onde de surface sur le glissement de Saint-Guillaume. Modèles de Vs en fonction de la profondeur et de l'erreur (échelle de couleur) pour les ondes de surface (a) et pour le bruit sismique (c). Surimposition de la courbe de dispersion avec les modèles dérivée des ondes de surface (b) et du bruit de fond sismique (d). Surimposition de la courbe de dispersion issue du réseau de bruit de fond sismique et de la carte de semblance des ondes de surface.

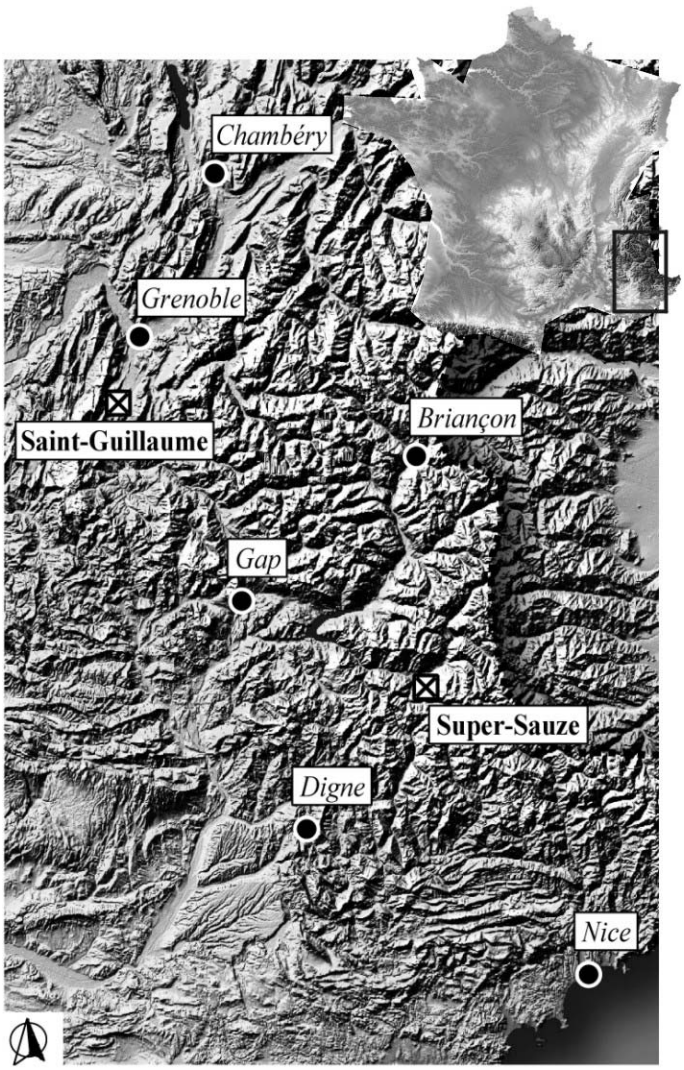
Chambéry
Grenoble
Saint-Guillaume
Briançon
Gap
Super-Sauze
Digne
Nice

Figure 1

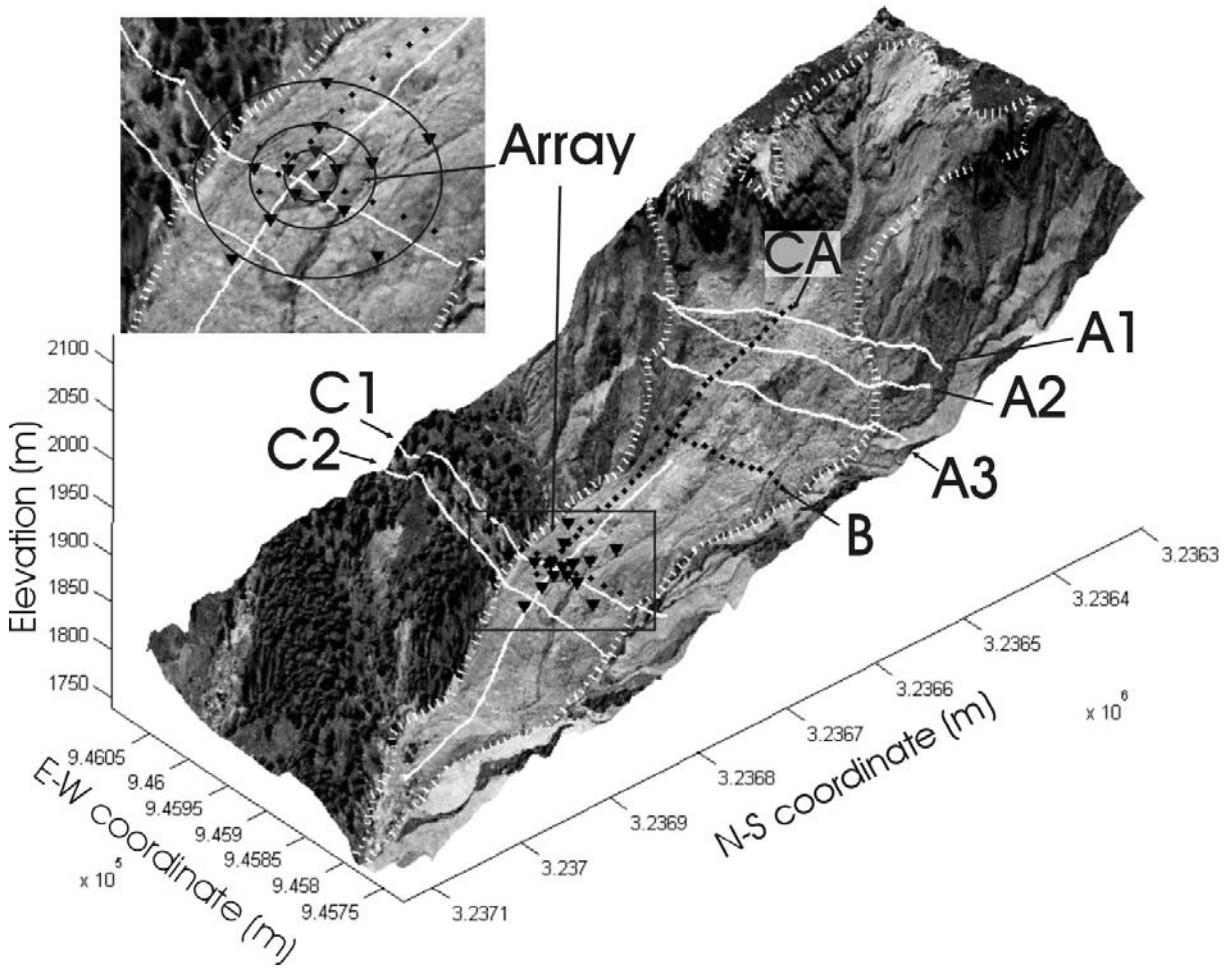
Array
CA
A1
A2
A3
B
C1
C2
Elevation (m)
2100
2050
2000
1950
1900
1850
1800
1750
E-W coordinate (m)
x 10^5
9.4605
9.46
9.4595
9.459
9.4585
9.458
9.4575
N-S coordinate (m)
x 10^6
3.2363
3.2364
3.2365
3.2366
3.2367
3.2368
3.2369
3.237
3.2371

Figure2

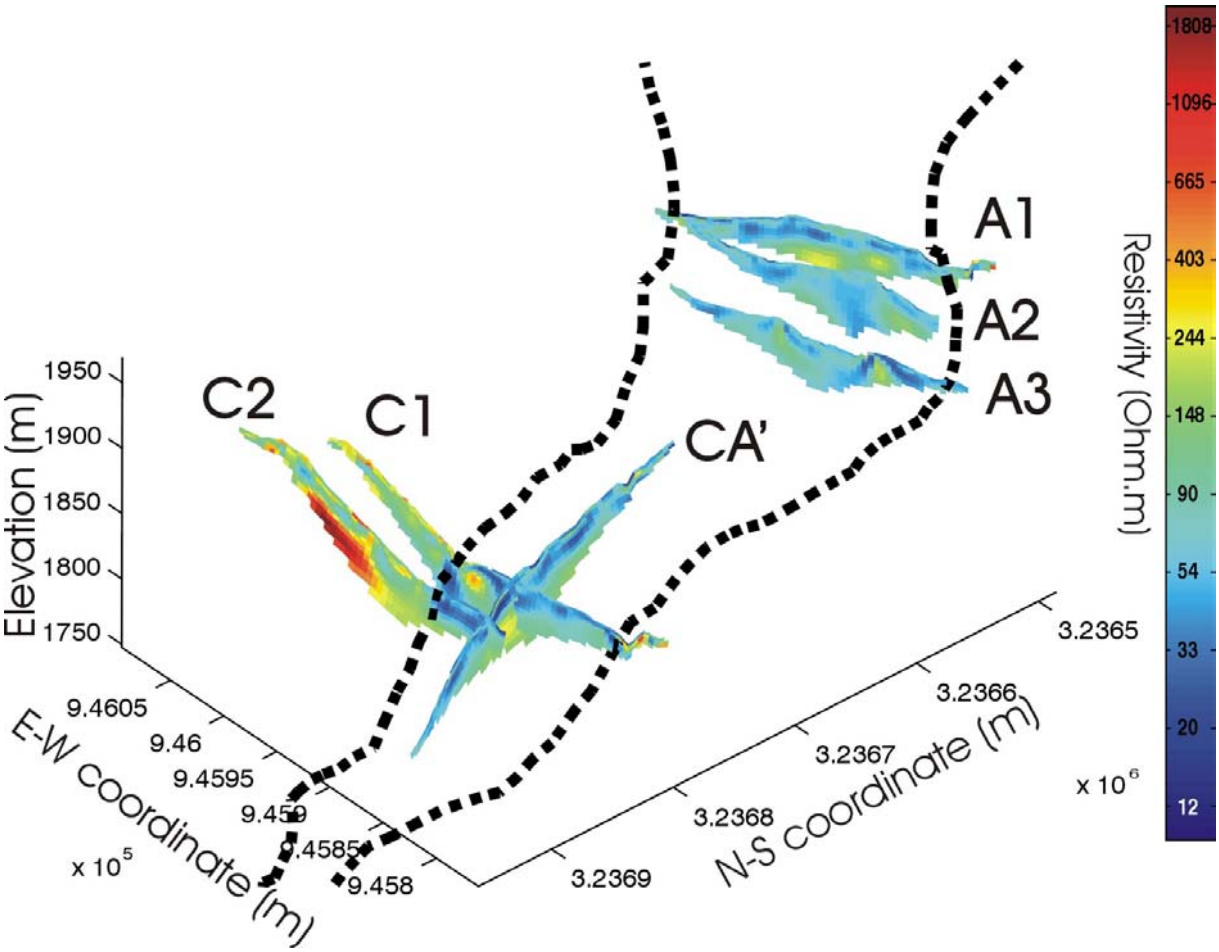
A1
A2
A3
C2
C1
CA'
Elevation (m)
1950
1900
1850
1800
1750
E-W coordinate (m)
x 10^5
9.4605
9.46
9.4595
9.459
9.4585
9.458
N-S coordinate (m)
x 10^6
3.2365
3.2366
3.2367
3.2368
3.2369
Resistivity (Ohm.m)
1808
1096
665
403
244
148
90
54
33
20
12

1

2

3 **Figure 3**

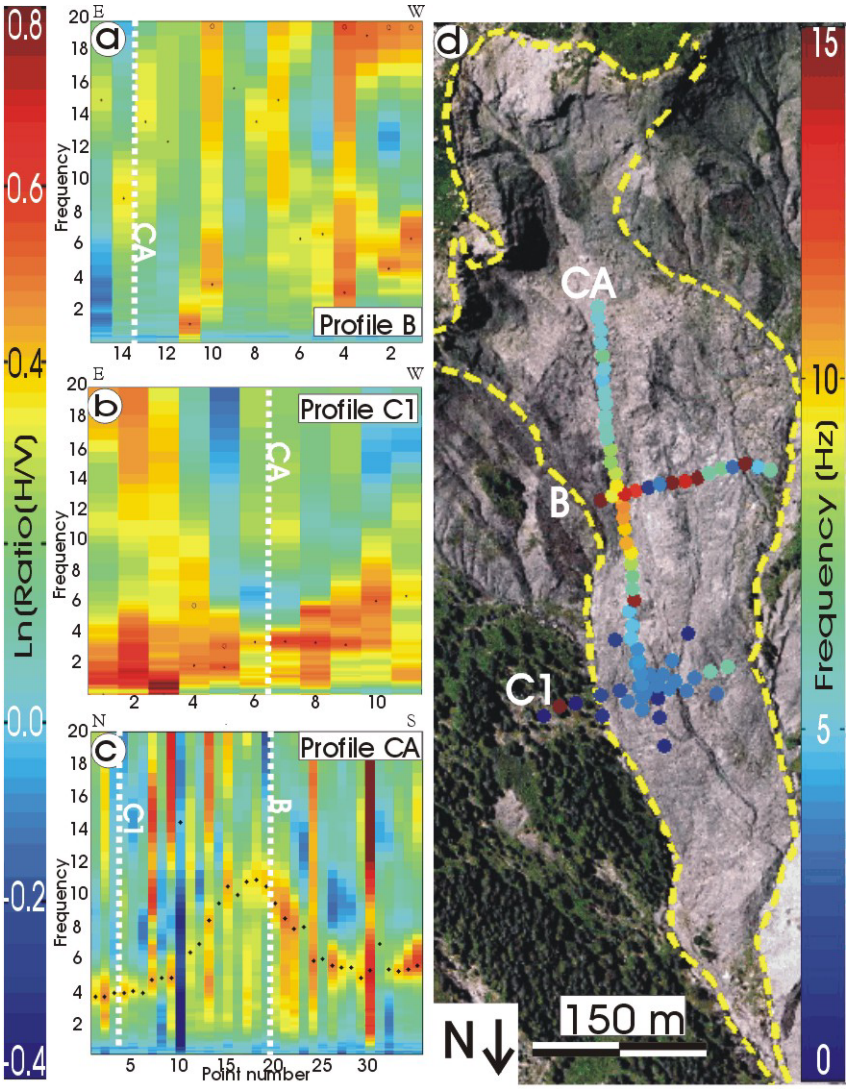
Ln(Ratio(H/V))
0.8
0.6
0.4
0.0
-0.2
-0.4
a
Profile B
CA
E
W
Frequency
b
Profile C1
CA
c
Profile CA
C1
B
N
S
Point number
d
CA
B
C1
150 m
N
Frequency (Hz)
15
10
5
0

Figure 4

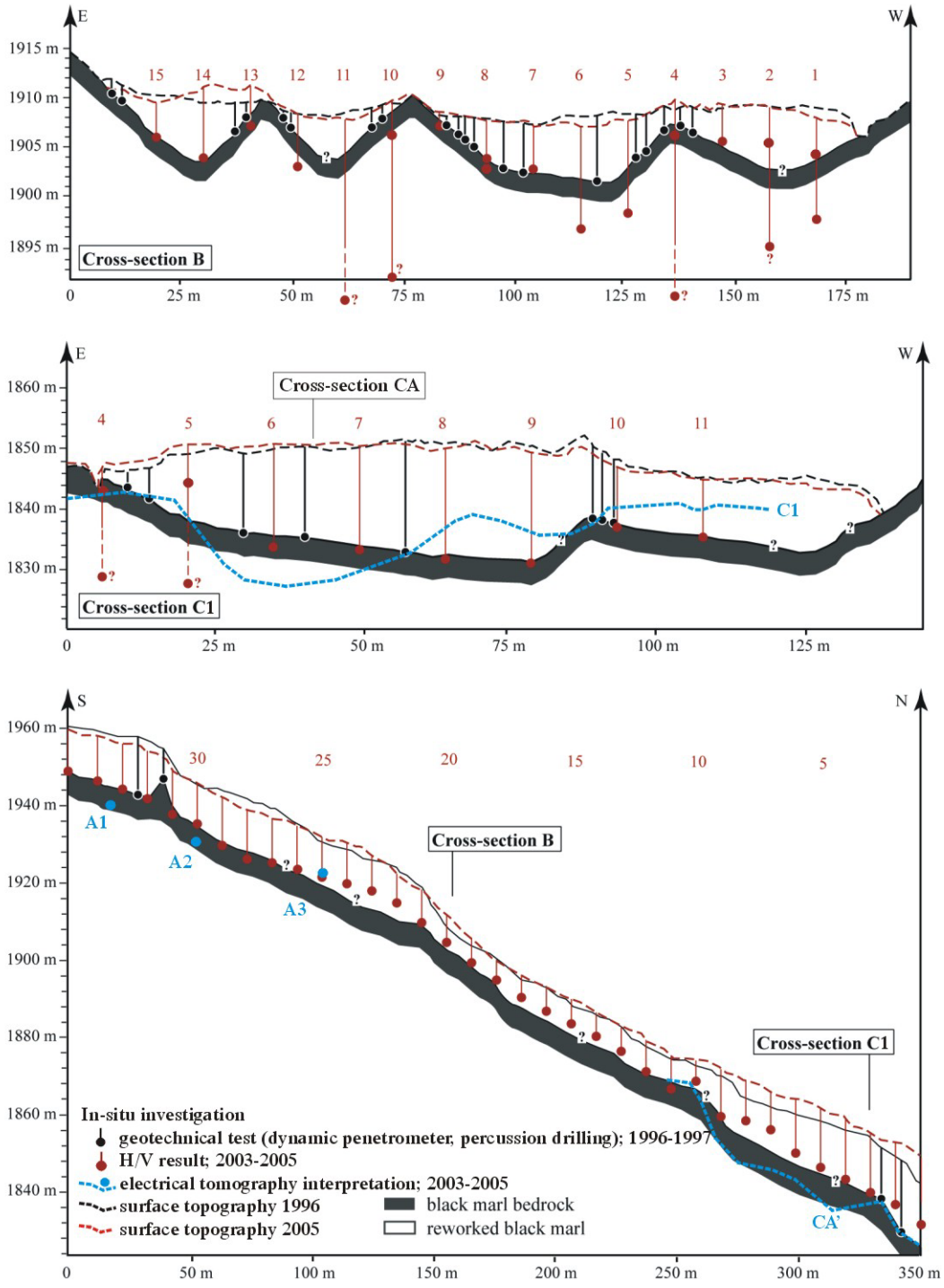
E
W
1915 m
1910 m
1905 m
1900 m
1895 m
15 14 13 12 11 10 9 8 7 6 5 4 3 2 1
Cross-section B
0 25 m 50 m 75 m 100 m 125 m 150 m 175 m
E
W
1860 m
1850 m
1840 m
1830 m
Cross-section CA
4 5 6 7 8 9 10 11
C1
Cross-section C1
0 25 m 50 m 75 m 100 m 125 m
S
N
1960 m
1940 m
1920 m
1900 m
1880 m
1860 m
1840 m
30 25 20 15 10 5
A1
A2
A3
Cross-section B
Cross-section C1
CA'
In-situ investigation
geotechnical test (dynamic penetrometer, percussion drilling); 1996-1997
H/V result; 2003-2005
electrical tomography interpretation; 2003-2005
surface topography 1996
surface topography 2005
black marl bedrock
reworked black marl
0 50 m 100 m 150 m 200 m 250 m 300 m 350 m

Figure 5

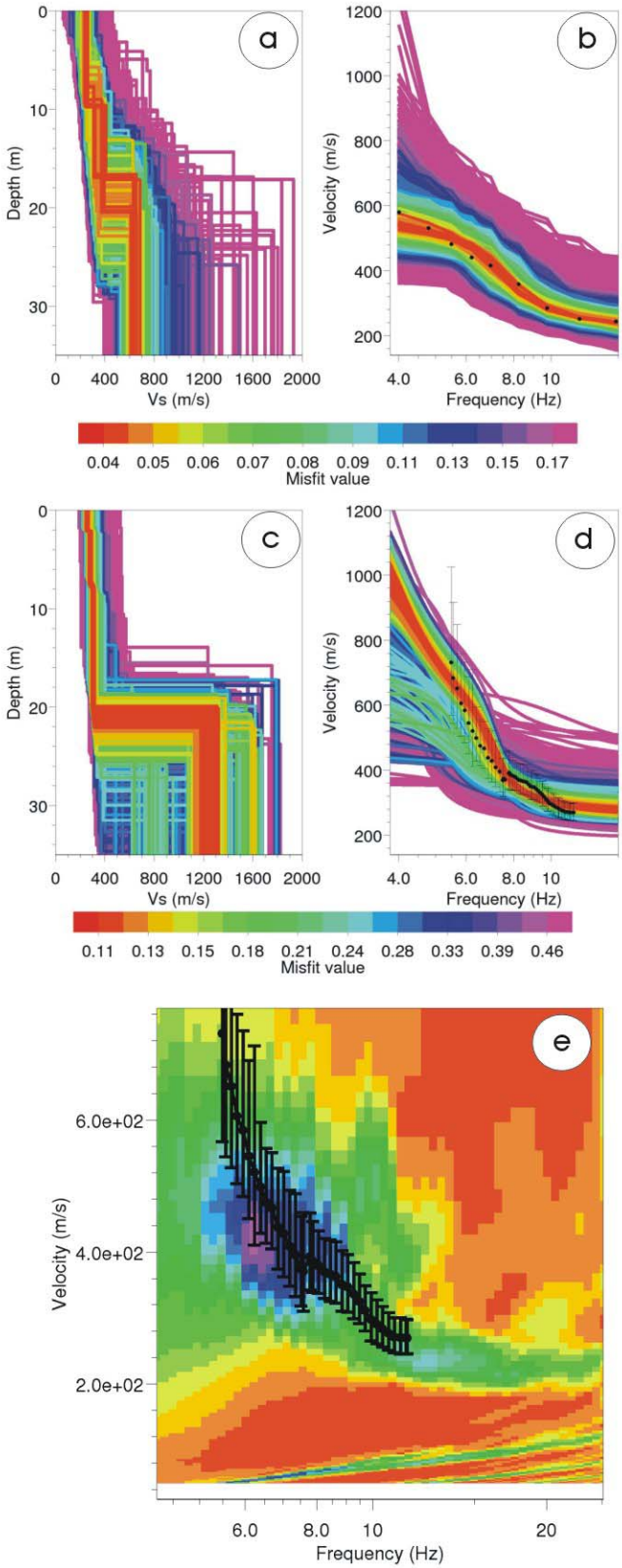
a
b
c
d
e
Depth (m)
Vs (m/s)
Velocity (m/s)
Frequency (Hz)
Misfit value
0.04 0.05 0.06 0.07 0.08 0.09 0.11 0.13 0.15 0.17
0.11 0.13 0.15 0.18 0.21 0.24 0.28 0.33 0.39 0.46
6.0e+02
4.0e+02
2.0e+02

1

2

3 **Figure 6**

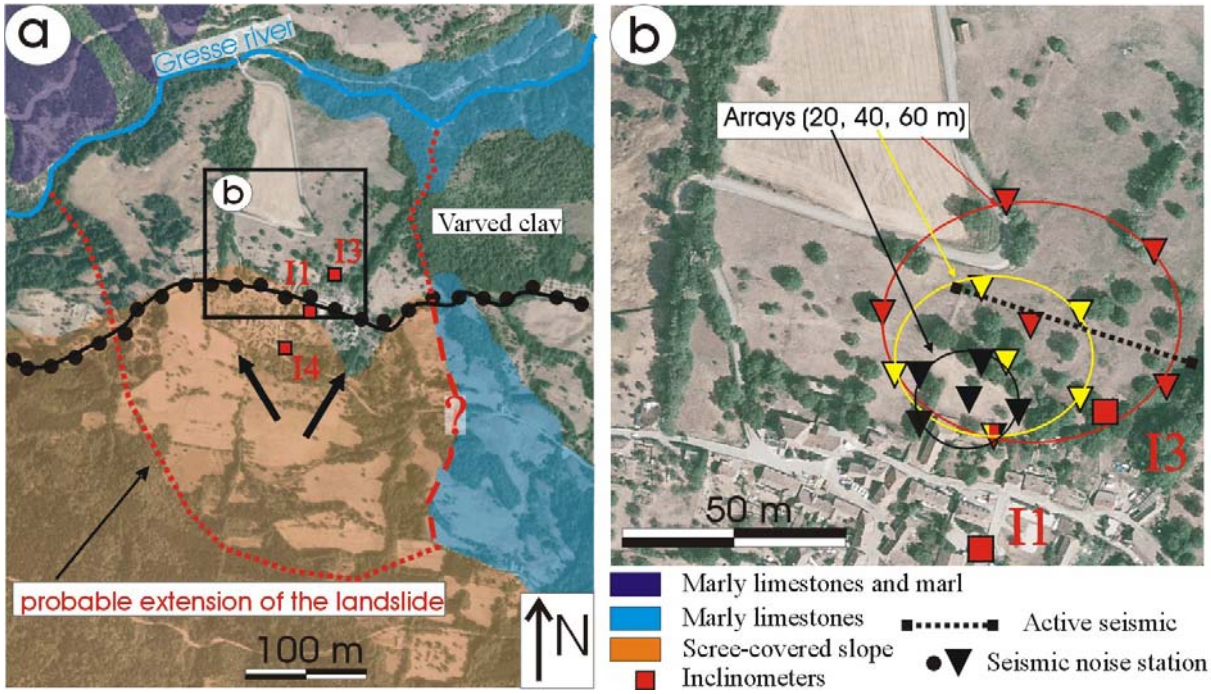
a
Gresse river
b
Varved clay
I1
I3
I4
?
probable extension of the landslide
100 m
N
b
Arrays (20, 40, 60 m)
50 m
I3
I1
Marly limestones and marl
Marly limestones
Scree-covered slope
Inclinometers
Active seismic
Seismic noise station

Figure 7

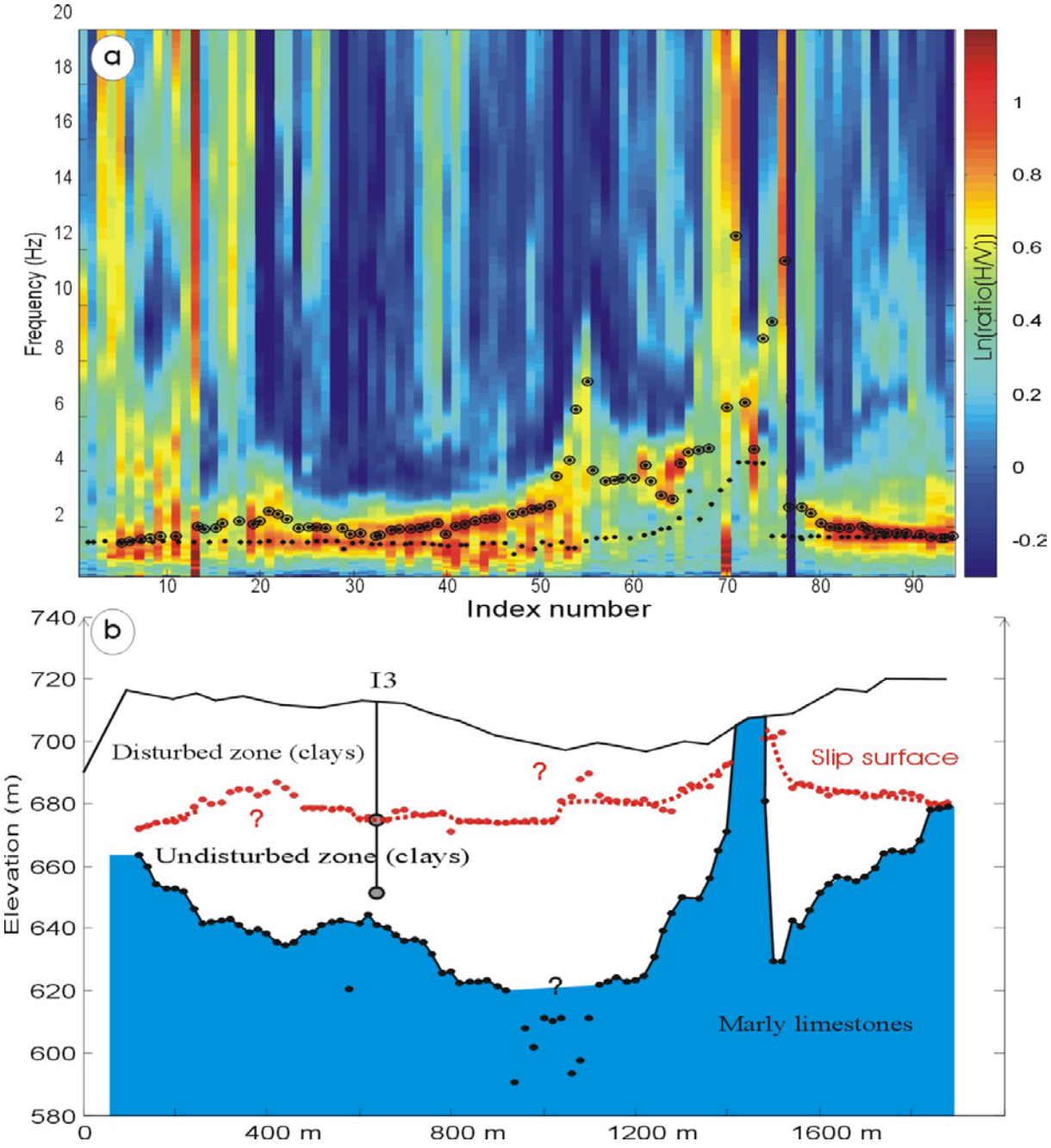
a
Frequency (Hz)
Index number
Ln(ratio(H/V))
b
Elevation (m)
I3
Disturbed zone (clays)
Undisturbed zone (clays)
Slip surface
Marly limestones
?
0
400 m
800 m
1200 m
1600 m

Figure 8

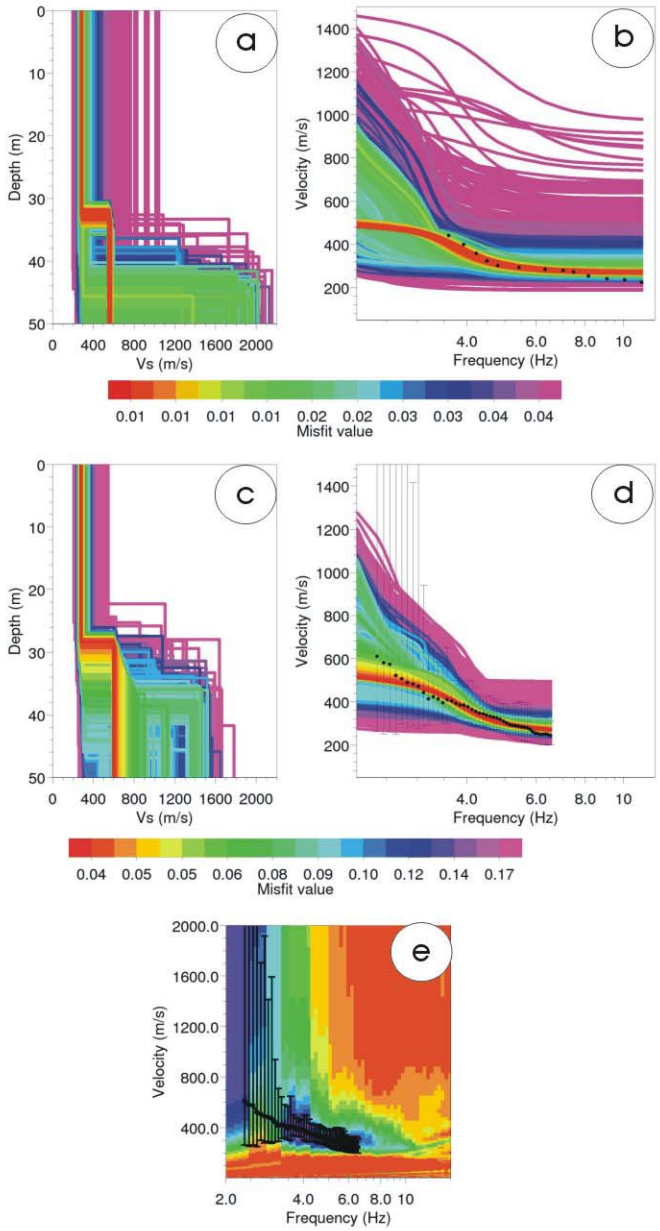
a
b
c
d
e
Depth (m)
Vs (m/s)
Velocity (m/s)
Frequency (Hz)
Misfit value
0.01 0.01 0.01 0.01 0.02 0.02 0.03 0.03 0.04 0.04
0.04 0.05 0.05 0.06 0.08 0.09 0.10 0.12 0.14 0.17

Figure9